American Mineralogist, Volume 87, pages 931–939, 2002

# High-pressure single-crystal X-ray and powder neutron study of F,OH/OD-chondrodite: Compressibility, structure, and hydrogen bonding

ALEXANDRA FRIEDRICH,[1,*] GEORGE A. LAGER,[2] PETER ULMER,[3] MARTIN KUNZ,[1,†] AND WILLIAM G. MARSHALL[4]

[1]Laboratorium für Kristallographie, ETH, Sonneggstrasse 5, CH-8092 Zürich, Switzerland
[2]Department of Geography and Geosciences, University of Louisville, Louisville, Kentucky 40292-0001, U.S.A.
[3]Institut für Mineralogie und Petrographie, ETH, Sonneggstrasse 5, CH-8092 Zürich, Switzerland
[4]ISIS Facility, CLRC Rutherford Appleton Laboratory, Chilton, Didcot OX11 0QX, U.K.

## ABSTRACT

The crystal structure of a natural F-bearing chondrodite [$Mg_{4.64}Fe_{0.28}Mn_{0.014}Ti_{0.023}(Si_{1.01}O_4)_2F_{1.16}OH_{0.84}$; $a = 4.7328(1)$, $b = 10.2749(2)$, $c = 7.8756(1)$ Å, $\alpha = 109.065(1)°$; space group $P2_1/b$ ($a$ unique)] from the Tilly Foster mine (Brewster, New York) and the structure of a deuterated synthetic analogue [$Mg_5(SiO_4)_2F_{1.10}OD_{0.90}$] were refined at high pressure using single-crystal X-ray and time-of-flight neutron powder diffraction data, respectively. The isothermal equation of state was determined from single-crystal high-precision X-ray diffraction measurements of unit-cell parameters as a function of pressure up to 9.63(1) GPa. A third-order Birch-Murnaghan equation-of-state fit to pressure-volume data results in $V_0 = 362.00(2)$ Å$^3$, $K_{0,T} = 117.0(4)$ GPa and $K_T' = 5.6(1)$. The larger value of $K_{0,T}$ relative to that determined for the OH end-member confirms that F makes the chondrodite structure less compressible. The axial compressibilities behave anisotropically with fitted parameters $a_0 = 4.73282(9)$ Å, $K(a)_0 = 458(3)$ GPa, and $K(a)' = 28.9(9)$; $b_0 = 10.2759(3)$ Å, $K(b)_0 = 298(1)$ GPa, and $K(b)' = 13.4(4)$; $c_0 = 7.8759(2)$ Å, $K(c)_0 = 316(2)$ GPa, and $K(c)' = 16.7(5)$. X-ray structural investigations at 0.0001, 4.952(7), and 9.550(7) GPa in a diamond-anvil cell reveal a complex compression mechanism. The greatest changes with pressure occur in the M2 octahedra, which are located at the flexion points of the octahedral chain. These octahedra have the longest bonds at ambient conditions due to cation-cation repulsion, which displaces the cation from the centroid of the octahedron. The application of pressure overcomes the effect of cation-cation repulsion inducing a strong bond-length compression. The neutron powder data were collected at 0.0001, 1.26(1), 2.89(2), 3.87(1), 5.27(2), and 7.04(2) GPa in the Paris-Edinburgh cell using a new gasket design and a fluid pressure medium. Changes in the O-D···O/F hydrogen bond geometry with pressure can be interpreted in terms of a rotation of the OD vector and a reduction in the degree of static disorder associated with the hydrogen bond acceptor/donor site. These new crystallographic data are discussed in terms of corresponding spectroscopic measurements reported recently in the literature.

## INTRODUCTION

Structurally incorporated water (hydrogen) in high-pressure phases can have a dramatic effect on mantle processes. Dehydration and rapid phase changes at depth have been linked to the localization of stress and the generation of deep-focus earthquakes along subduction zones (Lundgren and Giardini 1994). Furthermore, it has been suggested that dehydration-rehydration reactions during subduction of oceanic lithosphere are an important mechanism for transporting and recycling water between crust and mantle (Stalder and Ulmer 2001). In nominally anhydrous minerals, such as olivine, trace amounts of water in the form of OH defects can significantly affect rheological properties (Hirth and Kohlstedt 1996). Recent studies on hydrous phases have shown that their stability is strongly affected by hydrogen bonding. In the $MgO-SiO_2-H_2O$ system, phase transitions in phase B at high pressure have been related to variations in hydrogen bonding (Faust and Williams 1996). On the other hand, the strengthening of hydrogen bonds during compression of brucite, $Mg(OH)_2$, suggests that hydrogen stabilizes certain phases in the mantle (Parise et al. 1994; Catti et al. 1995).

Within the $MgO-SiO_2-H_2O$ system, the majority of studies have focused on the so-called alphabet phases (A, B, etc.). The humite-group minerals, which may be important hydrous phases in the upper mantle, have received considerably less attention. Unlike most synthetic phases in the $MgO-SiO_2-H_2O$ system, humites have natural analogues that are associated with rocks of possible mantle origin (e.g., McGetchin et al. 1970; Aoki et al. 1976; Dymek et al. 1988). In addition, the hydrogen-atom environment in humites can be used as a model for the local structural environment of OH defects in mantle olivine

---

* E-mail: a.friedrich@kristall.erdw.ethz.ch

† Present address is Department of Earth Sciences, University of Basel, Bernoullistrasse 30, CH-4056 Basel, Switzerland.

0003-004X/02/0007–931$05.00

(Kitamura et al. 1987; Miller et al. 1987; Sykes et al. 1994; Risold et al. 2001).

Humite minerals can be represented by the general formula $n[Mg_2SiO_4]\cdot[M_{1-x}Ti_x(F,OH)_{2-2x}O_{2x}]$, where M is primarily Mg with minor amounts of $Fe^{2+}$, Mn, Ni, Ca, Zn, Cu, $0 < x < 0.5$ and $n = 1, 2, 3$ and 4 for norbergite, chondrodite, humite, and clinohumite, respectively. Within the humite group, clinohumite and chondrodite are the most relevant to upper mantle processes because of their high *P-T* stability and association with mantle-derived rocks. The presence of fluorine increases the thermal stability of both chondrodite and clinohumite (Duffy and Greenwood 1979; Engi and Lindsley 1980; Weiss 1997; Stalder and Ulmer 2001) and has a significant effect on physical properties, such as compressibility. Most F-bearing humites occur in metamorphosed limestones and dolomites. However, F-bearing titanian clinohumites have been found in ultramafic rocks formed by high-pressure metamorphism (Evans and Trommsdorff 1983). Taskaev and Ilupin (1990) also describe an F-bearing, essentially Ti-free clinohumite in a Siberian kimberlite. The clinohumite is associated with K-richterite and garnet which suggests pressures >6 GPa and depths >180 km.

In this study, the compressibility and crystal structure of F-bearing chondrodite have been determined using in situ high-pressure single-crystal X-ray and powder neutron diffraction methods. X-ray data were collected for a natural (F,OH)-chondrodite (Tilly Foster Mine, Brewster, New York); a synthetic deuterated analog was used in the neutron study. The X-ray sample was cut from the same crystal used by Friedrich et al. (2001) in their single-crystal neutron study of chondrodite and clinohumite. Because of the complexity of the structure, X-rays were used to precisely locate the atoms that constitute the humite framework whereas neutrons provided information on the deuterium-atom environment at high pressure. Results are discussed in terms of existing bulk moduli data (Faust and Knittle 1994; Kuribayashi et al. 1998; Sinogeikin and Bass 1999; Ross and Crichton 2001) and high-pressure spectroscopic measurements (Williams 1992; Cynn and Hofmeister 1994; Hofmeister et al. 1999; Lin et al. 1999; Kuribayashi et al. 1998) to (1) determine the effect of the $F(OH)_{-1}$ substitution on the bulk modulus; (2) characterize the mechanism of compression; and (3) correlate crystallographic and spectroscopic data on hydrogen bonding at high pressure.

## EXPERIMENTAL METHODS

### Synthesis

Polycrystalline samples of (OD,F)-chondrodite totaling 500 mg were synthesized from stoichiometric oxide and fluoride mixtures in five experiments (68–108 h) using a piston-cylinder apparatus (1273 K, 2.0 GPa). The mixtures were prepared from reagent grade MgO and $SiO_2$ fired at 1373 K and $MgF_2$ dried at 673 K, following a procedure similar to that described by Duffy and Greenwood (1979). The amount of $MgF_2$ was adjusted to 1.16 F per formula unit (pfu) to produce synthetic samples with the same F content as the natural chondrodite material, i.e., $X_{OD} = 0.42$ where $X_{OD} = OD / (F + OD)$. We assumed initially (see below) that F enters the chondrodite structure and that the coexisting fluid is essentially $D_2O$ with minor MgO and $SiO_2$ in solution.

In all experiments 2.6–3.5 wt% excess $D_2O$ (total amount of 4.8–5.7 wt% $D_2O$) was added to the oxide-fluoride mix, which was then sealed in gold capsules with an outer diameter of 4.0 mm. Experiments were performed in an end-loaded piston cylinder apparatus with piston diameters of 14 mm. Assemblies consisted of NaCl-Pyrex-MgO and were calibrated with the following reactions/phase transitions: fayalite + quartz = orthoferrosilite at 1.41 GPa and 1273 K (Bohlen et al. 1980) and quartz = coesite at 3.2 GPa and 1473 K (Bose and Ganguly 1995). Runs were terminated by near isobaric quench with quench rates between 200–400 K/s.

The recovered charges were weighed and pierced; the presence of fluid was confirmed by strong "bubbling" upon piercing and weight loss during subsequent heating. Examination of the experimental products by X-ray powder diffraction and Raman micro-spectroscopy revealed the presence of minor amounts of (OD,F)-humite $Mg_7(SiO_4)_3(OD,F)_2$, in addition to (OD,F)-chondrodite, in all but two of the samples. The F-contents determined from the *d*-spacing of the $\bar{1}12$ reflection in the powder diffraction patterns (Duffy and Greenwood 1979) were within 1 e.s.d. of the targeted value of 1.16 F pfu.

### Single-crystal X-ray compressibility measurements

Two sets of unit-cell data (16 measurements) for the Tilly Foster chondrodite were obtained as a function of pressure using single-crystal X-ray diffraction methods. An untwinned single-crystal fragment (100 × 100 × 40 μm) of chondrodite was loaded together with a quartz crystal as pressure standard (Angel et al. 1997) into an ETH-designed diamond-anvil cell (Miletich et al. 2000). The sample hole [250(5) μm; pre-indented to a thickness of 92 μm] was drilled in an Inconel steel gasket using a spark-erosion drilling machine. The diamond anvils had a culet face diameter of 0.6 mm. A 4:1 methanol-ethanol mixture was used as the pressure-transmitting medium. The first data set was measured to a maximum pressure of 6.9 GPa. A second data set was collected to 9.6 GPa with a smaller hole [200(5) μm; pre-indented to a thickness of 98 μm] drilled in a T301-steel gasket. The measurements were performed at room temperature with a HUBER four-circle diffractometer using unfiltered and non-monochromatized Mo X-ray radiation (50 kV, 40 mA). Unit-cell parameters of both the quartz and the chondrodite crystals were obtained by applying the diffracted-beam centering technique (King and Finger 1979) to correct for crystal-offset errors. For chondrodite, 30–34 accessible reflections with $11.7° \leq 2\theta \leq 35.5°$ were used. Pressure calibration was based on 13–16 quartz reflections with $9° \leq 2\theta \leq 32°$. The lattice parameters constrained to monoclinic symmetry were obtained by a vector least-squares fit to the corrected reflection positions.

To obtain compressibilities, *P-V*, *P-a*, *P-b*, and *P-c* data were fitted with a third-order Birch-Murnaghan equation of state (EOS) using a fully weighted least-squares procedure. The pressures were determined from the refined unit-cell parameters and the EOS parameters of quartz (Angel et al. 1997). Since the same crystal was used in both loadings, the two sets of *P-V* data were merged and fitted as a single data set.

## Single-crystal X-ray intensity data collection and refinement

X-ray intensity data collection was performed at ambient temperature and pressures of 0.0001, 4.952, and 9.550 GPa using an Enraf Nonius CAD4 four-circle diffractometer with graphite-monochromatized Mo$K\alpha$ radiation. The intensity measurements were carried out with ω-scans (scan range: 0.80° + 0.35° tanθ; aperture = 3.2 + 0.35) at the position of least attenuation by the pressure cell, according to the fixed-φ technique (Finger and King 1978). Hence, the reflection accessibility was maximized and attenuation of the X-ray beams by the pressure-cell components was minimized. All symmetry-allowed accessible reflections within a full sphere were collected up to the maximum θ angle. Intensity data were obtained from the scan data using a modified Lehmann-Larsen algorithm (Grant and Gabe 1978). Intensities were corrected for Lorentz and polarization effects and absorption of the X-ray beam by the diamond and beryllium components of the pressure cell using a modified version of ABSORB (Burnham 1966). Symmetry equivalent reflections were averaged in Laue symmetry $2/m$ following the criteria recommended by Blessing (1987).

The structure refinements were carried out in space group $P2_1/b$ (*a* unique) with RFINE99, a development version of RFINE4 (Finger and Prince 1975 as modified by R.J. Angel, personal communication). The atomic coordinates from Friedrich et al. (2001) were used as starting parameters in the refinements. The H atom was excluded from the refinement model. The coefficients for the neutral atom scattering factors and dispersion corrections were taken from the *International Tables for Crystallography* (Maslen et al. 1992; Creagh and McAuley 1992). The final refinements of the high-pressure data sets were carried out with isotropic displacement parameters for all atoms. The F:O ratio was fixed based on the neutron site-occupancy refinement (Friedrich et al. 2001). The site occupancy of M1 was refined with the constraint Σ(Fe + Mg) = 1. Several reflections were excluded from the refinements due to overlapping diamond reflections, their λ/2 artifacts, and high and asymmetric backgrounds (weak reflections).

## Powder neutron diffraction measurements

About 170 mg of powdered sample of pure synthetic deuterated F-bearing chondrodite were loaded into a type V4b Paris-Edinburgh high-pressure cell (Besson et al. 1992) equipped with standard profile WC/Ni-binder anvils. The sample was confined between the anvils with a soft-metal-encapsulated (SME), single-toroid gasket consisting of a null-scattering Ti-Zr alloy (Marshall and Francis 2002). A standard 4:1 by volume mixture of deuterated methanol and ethanol was used as the pressure-transmitting medium. Oil pressure in the in situ ram was raised using a hand-operated hydraulic pump.

Time-of-flight (TOF) neutron powder-diffraction data were collected at 0.0001, 1.26, 2.89, 3.87, 5.27, and 7.04 GPa with the PEARL/HiPr diffractometer at the U.K. pulsed spallation source, ISIS. Integrated ISIS currents ranged from 1493 μA·h (~8.5 h at 175 μA proton current) to 2093 μA·h (~12 h) for the non-ambient experiments. Because of limited neutron beam time, data were collected at ambient pressure in the pressure cell for only a little more than 1 h (193 μA·h). Nevertheless, this run was important in that it provided the ambient unit-cell volume from which it was possible to obtain the non-ambient run pressures from the EOS determined from the single-crystal X-ray data.

The overall *d*-spacing focused time-of-flight powder diffraction pattern obtained using the PEARL/HiPr 90° detector bank was corrected for neutron attenuation by the anvil and gasket materials and normalized to the incident spectrum using a local routine. Rietveld (1969) profile analysis for multiple-phase samples (chondrodite, WC, Ni), as coded in the General Structure Analysis System (GSAS) (Larson and Von Dreele 1994), was used for the structure refinements. Although the WC anvils were shielded with cadmium foil, a small amount of contaminant Bragg scattering from the anvil materials was observed in all profiles. Starting parameters for the refinements were taken from Friedrich et al. (2001). Due to the new gasket design and the use of the fluid pressure medium, no significant peak broadening and hence no strain within the sample was observed at increasing pressure (Fig. 1).

The value of the GSAS diffractometer constants DIFC, DIFA and ZERO were determined from the TOF diffraction pattern of a standards sample with accurately known unit-cell parameters, in this case NBS Si (SRM 640b).

A total of 57–60 variables were refined at non-ambient pressures and 17 variables at ambient pressure. Refinements included 3403–3550 Bragg reflections over the *d*-spacing range $0.5 < d < 4.14$ Å. The TOF peak profile was modeled with an exponential pseudovoigt function (function 3; Larson and Von Dreele 1994), and the background with a standard 10-term cosine Fourier series (function 2; Larson and Von Dreele 1994). The D-site occupancy was refined at the lowest pressure with the constraint Σ(OD + F) = 1, and then fixed for the higher-pressure refinements. The D-site occupancies of the synthetic [0.45(5)] and natural chondrodite samples [0.42(1)] (Friedrich et al. 2001) are identical within 1 e.s.d. The structure refinements revealed unreasonably long Si-O bond lengths (~1.68

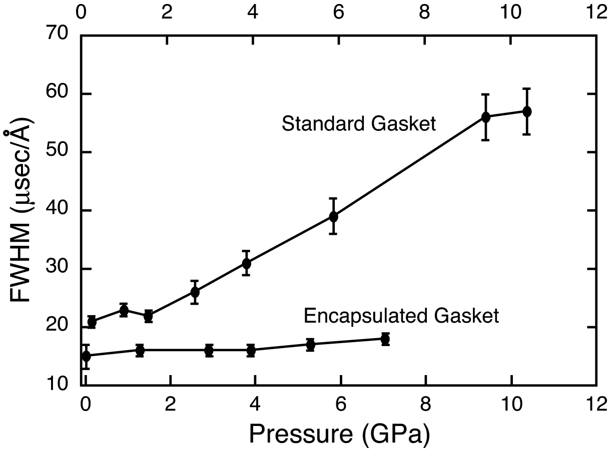

**FIGURE 1.** Peak widths (FWHM) for OD-chondrodite (standard gasket with fluorinert) and (OD,F)-chondrodite (SME gasket with 4:1 deuterated methanol:ethanol) from neutron powder diffraction patterns as a function of pressure. FWHM refers to the Gaussian part of the intrinsic sample contribution to the overall peak width.

Å), and a non-rigid behavior of the Si tetrahedron with pressure. One possible explanation for this observation is that the atomic coordinates of Si are less accurate because Si is the weakest neutron scatterer in the structure. To more realistically model the behavior of the tetrahedron, soft constraints (restraints) were applied to the Si-O bond distances based on the values determined in the X-ray refinements (Baerlocher 1993). The final refinement profile at 7.04 GPa is shown in Figure 2.

## RESULTS AND DISCUSSION

The variation in the unit-cell parameters measured by single-crystal X-ray diffraction methods as a function of pressure is summarized in Table 1. Equation-of-state parameters for the Tilly Foster chondrodite based on X-ray diffraction data are listed in Table 2. Details relating to the X-ray data collection and reduction and structural refinements are given in Table 3.

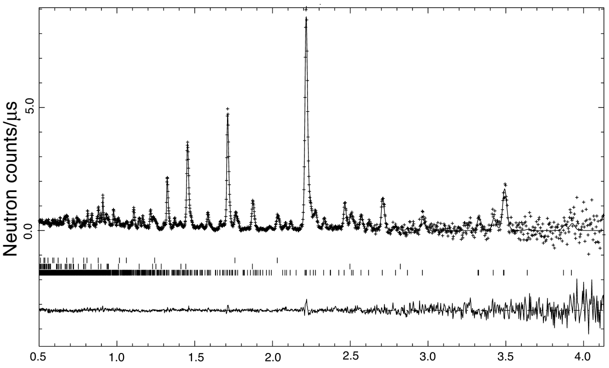

**FIGURE 2.** Observed (crosses) and calculated (line) TOF neutron powder diffraction patterns of (OD,F)-chondrodite at 7.04 GPa, and difference plot. Peak positions are given for Ni (top), WC (center) and chondrodite (bottom).

**TABLE 2.** Equation-of-state parameters for Tilly Foster chondrodite based on X-ray diffraction data

| | $V_0$ (Å$^3$), $a_0$ (Å) | $K_{0,T}$ (GPa) | $K'$ | $\chi^2$ |
|---|---|---|---|---|
| $V$ | 362.00(2) | 117.0(4) | 5.59(11) | 1.25 |
| $a$ | 4.73282(9) | 458(3) | 28.9(9) | 0.95 |
| $b$ | 10.2759(3) | 298(1) | 13.4(4) | 1.14 |
| $c$ | 7.8759(2) | 316(2) | 16.7(5) | 1.28 |

**TABLE 3.** Details on data reduction and agreement factors for the high-pressure X-ray structure refinements (Tilly Foster chondrodite)

| | 0.0001 GPa | 4.952 GPa | 9.550 GPa |
|---|---|---|---|
| prescan speed (°/min) | 4.120 | 2.06 | 5.493 |
| max. scan time (s) | 450 | 300 | 600 |
| standard reflections | (2 2 2) | (0 4 0) | (0 0 5) |
| for intensity control | (2 $\bar{2}$ 2) | (0 0 5) | (1 1 2) |
| | | (2 2 2) | (1 $\bar{1}$ 2) |
| max. θ (°) | 40 | 40 | 35 |
| voltage (kV) | 50 | 55 | 50 |
| current (mA) | 30 | 30 | 30 |
| total $\vert F\vert$ | 2433 | 2355 | 1953 |
| averaged $\vert F\vert$ | 891 | 858 | 721 |
| $\vert F\vert_{obs}$ ($F > 4\sigma$) | 361 | 412 | 358 |
| μ (Mo$K\alpha$) (cm$^{-1}$) | 13.95 | 15.07 | 15.52 |
| $t_{min}$ (%) | 29.2 | 29.0 | 30.7 |
| $t_{max}$ (%) | 38.9 | 38.8 | 38.7 |
| $R_{int}$ ($F > 4\sigma$) | 0.038 | 0.040 | 0.032 |
| $p_{var}$ | 34 | 34 | 34 |
| $R$ ($F > 4\sigma$) | 0.055 | 0.057 | 0.050 |
| $wR$ ($F > 4\sigma$) | 0.065 | 0.060 | 0.056 |
| GooF | 1.32 | 1.14 | 1.08 |

*Notes:* Only reflections passing the sigma criteria as given by Blessing (1987) are averaged. Transmission (t) includes both crystal absorption and absorption by DAC components.

$R = (\sum||F_o| - |F_c||)/(\sum|F_o|)$, where $F_o$ = observed structure factor and $F_c$ = calculated structure factor.

$wR = \{[\sum w(|F_o| - |F_c|)^2]/[\sum w|F_o|^2]\}^{-1/2}$, where $w = (\sigma_i^2 + P^2 F_o^2)^{-1}$ and $P$ = 0.035, 0.036, 0.037.

GooF = $\sqrt{\left(\sum w\left(F_o^2 - F_c^2\right)^2 / (n-p)\right)}$, where $n$ = number of averaged $|F|$ and $p = p_{var}$ = number of l.s. parameters.

**TABLE 1.** Variation of unit-cell parameters of the Tilly Foster chondrodite with pressure from single-crystal X-ray data

| $P$ (GPa) | Quartz | | Tilly Foster Chondrodite | | | | | |
|---|---|---|---|---|---|---|---|---|
| | $V$ (Å$^3$) | $N_{refl}$ | $a$ (Å) | $b$ (Å) | $c$ (Å) | $\alpha$ (°) | $V$ (Å$^3$) | $N_{refl}$ |
| | | | | **First data set** | | | | |
| 0.0001* | | | 4.7328(1) | 10.2749(2) | 7.8756(1) | 109.065(1) | 361.98(1) | 23 |
| 0.0001 † | 113.095(15) | | | | | | | |
| 0.068(6) | 112.888(7) | 15 | 4.7319(1) | 10.2729(2) | 7.8740(2) | 109.074(2) | 361.74(1) | 32 |
| 1.719(6) | 108.555(10) | 15 | 4.7160(1) | 10.2190(2) | 7.8352(2) | 109.049(1) | 356.92(1) | 31 |
| 3.565(7) | 104.771(8) | 15 | 4.6995(2) | 10.1629(4) | 7.7951(3) | 109.024(2) | 351.96(2) | 31 |
| 4.893(11) | 102.504(15) | 15 | 4.6888(3) | 10.1243(7) | 7.7677(5) | 109.015(4) | 348.62(3) | 31 |
| 5.730(10) | 101.222(13) | 14 | 4.6815(3) | 10.1009(6) | 7.7508(5) | 108.989(4) | 346.57(3) | 30 |
| 6.376(9) | 100.296(11) | 14 | 4.6767(3) | 10.0833(8) | 7.7396(6) | 108.982(5) | 345.13(4) | 31 |
| 6.933(11) | 99.537(13) | 14 | 4.6728(4) | 10.0689(10) | 7.7267(8) | 108.966(7) | 343.81(5) | 30 |
| | | | | **Second data set** | | | | |
| 0.0001* | | | 4.7328(1) | 10.2749(2) | 7.8756(1) | 109.065(1) | 361.98(1) | 23 |
| 0.0001 †‡ | 113.123(14) | 13 | 4.7328(2) | 10.2765(5) | 7.8760(4) | 109.081(3) | 362.01(3) | 32 |
| 1.139(6) | 109.976(10) | 15 | 4.7217(1) | 10.2383(3) | 7.8484(2) | 109.052(2) | 358.63(1) | 31 |
| 2.439(7) | 107.001(11) | 15 | 4.7094(4) | 10.1959(11) | 7.8189(8) | 109.033(7) | 354.91(6) | 32 |
| 4.319(9) | 103.472(12) | 15 | 4.6933(1) | 10.1402(3) | 7.7794(2) | 109.008(2) | 350.04(1) | 33 |
| 4.952(7) ‡ | 102.436(7) | 15 | 4.6881(3) | 10.1222(7) | 7.7660(5) | 108.989(5) | 348.47(4) | 32 |
| 4.979(6) | 102.393(6) | 15 | 4.6880(1) | 10.1219(2) | 7.7659(2) | 108.994(1) | 348.44(1) | 33 |
| 7.808(7) | 98.437(7) | 15 | 4.6664(3) | 10.0454(6) | 7.7131(5) | 108.957(4) | 341.95(3) | 34 |
| 9.550(7) ‡ | 96.405(6) | 15 | 4.65459(9) | 10.0033(2) | 7.6828(2) | 108.939(1) | 338.35(1) | 33 |
| 9.627(13) | 96.321(14) | 16 | 4.6538(2) | 10.0000(6) | 7.6804(4) | 108.933(4) | 338.09(3) | 6 |

*Note:* Space group $P2_1/b$ (unique axis $a$).

$N_{refl}$ = number of reflections used for the vector least-squares refinement of the unit-cell parameters.

* Crystal in air.

† Crystal in DAC without pressure-transmitting medium.

‡ Pressures at which intensity data were collected.

Atom positions and isotropic displacement parameters are listed in Table 4, while Table 5 shows selected bond distances and angles. Refined unit-cell parameters based on neutron data are given in Table 6. Atom positions and isotropic atomic displacement parameters from neutron powder diffraction data are presented in Table 7. Table 8 contains selected O-D···O/F interatomic distances and angles at high pressure.

## Compressibility data

The isothermal bulk modulus of the Tilly Foster chondrodite [$X_{OH} = 0.42$; $K_{0,T} = 117.0(4)$ GPa] determined by X-ray single-crystal diffraction is consistent with the bulk modulus [$K_S = 118(2)$ GPa] determined from Brillouin scattering of a sample from the same locality with $X_{OH} = 0.68$ (Sinogeikin and Bass 1999). Sinogeikin and Bass (1999) discussed the possibility that the OH content of their chondrodite sample is too high based on the uncertainties in the measurement of the F content by electron microprobe analysis and comparisons with published chemical analyses (Ribbe 1979, 1980). The neutron single-crystal refinement of the structure of Tilly Foster chondrodite (Friedrich et al. 2001) suggests a lower OH content for samples from this locality. Synthetic hydroxyl-chondrodite has a bulk modulus of $K_{0,T} = 115.5(6)$ GPa (Ross and Crichton 2001), which is slightly, but significantly smaller than $K_{0,T}$ of the F-bearing chondrodite. This result confirms that the chondrodite structure becomes more compressible with increasing OH content, which is consistent with the unit-cell volume increase associated with the substitution of the larger OH ion for F.

Faust and Knittle (1994) investigated the compressional behavior of a F-rich chondrodite with $X_{OH} = 0.27$, resulting in $K_{0,T} = 136(9)$ GPa and $K_T' = 3.7(4)$. These data were measured with synchrotron X-ray powder diffraction methods using a diamond-anvil cell. The errors are large due to the large uncertainties in pressure and unit-cell volume. The authors used no internal diffraction standard but only the ruby fluorescence technique for pressure determination, which is sensitive to small temperature variations. In addition, the unit-cell volumes were calculated from only eight reflections in the powder diffraction pattern. Hence, a fit of $K_T'$ is probably not reliable. If their data are refit with $K_T' \equiv 4.9–5.5$, the bulk moduli range from 118 to 125 GPa, which is in closer agreement with the results of this study and the single-crystal compression measurements of Ross and Crichton (2001). If the mean values of $K_{0,T}$ and $K_T'$ obtained by Faust and Knittle (1994) were correct, their EOS would be an indication of a strongly non-linear behavior of the elasticity as a function of F content, which seems unlikely. Kuribayashi et al. (1998) reported a bulk modulus of $K_{0,T} = 136(2)$ GPa with $K_T' \equiv 4$ for a F-bearing chondrodite using single-crystal X-ray diffraction. This value is similar to that

**TABLE 5.** Selected interatomic distances (Å) from X-ray structure refinements (Tilly Foster chondrodite)

| | 0.0001 GPa | 4.952 GPa | 9.550 GPa |
|---|---|---|---|
| M1-O1 (2×) | 2.092(8) | 2.072(6) | 2.035(7) |
| -O3 (2×) | 2.09(1) | 2.080(8) | 2.069(8) |
| -O4 (2×) | 2.13(1) | 2.099(7) | 2.072(8) |
| $V$(Å$^3$) | 11.78(8) | 11.52(6) | 11.16(6) |
| OQE | 1.036(4) | 1.031(3) | 1.028(3) |
| | | | |
| M2-O1 | 2.07(1) | 2.046(9) | 2.029(9) |
| -O2 | 2.25(1) | 2.182(8) | 2.159(8) |
| -O3 | 2.06(1) | 2.029(7) | 1.991(8) |
| -O3 | 2.20(1) | 2.161(7) | 2.130(8) |
| -O4 | 2.15(1) | 2.123(9) | 2.08(1) |
| -O5 | 2.057(8) | 2.027(6) | 2.011(6) |
| $V$(Å$^3$) | 12.43(8) | 11.88(5) | 11.46(6) |
| OQE | 1.026(5) | 1.022(4) | 1.019(4) |
| | | | |
| M3-O1 | 2.199(9) | 2.161(7) | 2.139(7) |
| -O2 | 2.01(1) | 1.982(8) | 1.961(8) |
| -O2 | 2.11(1) | 2.091(8) | 2.081(8) |
| -O4 | 2.15(1) | 2.082(8) | 2.077(8) |
| -O5 | 2.01(1) | 2.003(8) | 1.966(8) |
| -O5 | 2.055(9) | 2.026(7) | 2.007(7) |
| $V$(Å$^3$) | 11.81(6) | 11.33(5) | 11.03(5) |
| OQE | 1.02(1) | 1.018(9) | 1.017(9) |
| | | | |
| Si1-O1 | 1.61(1) | 1.612(9) | 1.61(1) |
| -O2 | 1.62(1) | 1.618(8) | 1.627(7) |
| -O3 | 1.61(1) | 1.617(7) | 1.628(8) |
| -O4 | 1.626(6) | 1.612(5) | 1.605(5) |
| $V$(Å$^3$) | 2.13(2) | 2.12(2) | 2.13(2) |
| TQE | 1.011(9) | 1.012(7) | 1.012(7) |
| | | | |
| O5···O5 | 2.954(9) | 2.895(7) | 2.866(7) |
| O5···O1 | 2.98(1) | 2.914(9) | 2.900(9) |

*Notes:* The octahedral (OQE) and tetrahedral (TQE) quadratic elongation is given after Robinson et al. (1971).

**TABLE 6.** Unit-cell parameters of synthetic (OD,F)-chondrodite from neutron powder Rietveld refinements

| $P$(GPa) | $a$ (Å) | $b$ (Å) | $c$ (Å) | $\alpha$ (°) | $V$(Å$^3$) |
|---|---|---|---|---|---|
| 0.0001 | 4.7314(4) | 10.262(2) | 7.866(1) | 109.14(2) | 360.81(4) |
| 1.26(1) | 4.7179(2) | 10.2247(7) | 7.8290(7) | 109.01(1) | 357.06(1) |
| 2.89(2) | 4.7024(2) | 10.1742(7) | 7.7938(8) | 109.00(1) | 352.56(2) |
| 3.87(1) | 4.6939(2) | 10.1458(7) | 7.7722(7) | 108.98(1) | 350.00(1) |
| 5.27(2) | 4.6827(2) | 10.1055(7) | 7.7449(7) | 108.98(1) | 346.58(2) |
| 7.04(2) | 4.6688(2) | 10.0589(7) | 7.7127(8) | 108.98(1) | 342.51(2) |

*Note:* Space group $P2_1/b$ (unique axis $a$).

**TABLE 4.** Atom positions and isotropic displacement parameters from X-ray structure refinements (Tilly Foster chondrodite)

| | 0.0001 GPa | | | | 4.952 GPa | | | | 9.550 GPa | | | |
|---|---|---|---|---|---|---|---|---|---|---|---|---|
| | $x$ | $y$ | $z$ | $U_{iso}$ | $x$ | $y$ | $z$ | $U_{iso}$ | $x$ | $y$ | $z$ | $U_{iso}$ |
| M1 | 1/2 | 0 | 1/2 | 0.009(4) | 1/2 | 0 | 1/2 | 0.010(3) | 1/2 | 0 | 1/2 | 0.010(3) |
| M2 | 0.0115(6) | 0.1731(7) | 0.3076(5) | 0.008(2) | 0.0097(5) | 0.1746(5) | 0.3054(4) | 0.008(2) | 0.0106(5) | 0.1748(6) | 0.3054(4) | 0.009(2) |
| M3 | 0.4922(6) | 0.8868(7) | 0.0783(6) | 0.010(2) | 0.4917(5) | 0.8871(6) | 0.0791(4) | 0.009(2) | 0.4924(5) | 0.8885(6) | 0.0800(5) | 0.010(2) |
| Si | 0.0773(6) | 0.1432(7) | 0.7051(5) | 0.0085(5) | 0.0760(5) | 0.1441(5) | 0.7045(4) | 0.008(2) | 0.0754(5) | 0.1444(5) | 0.7038(4) | 0.010(2) |
| O1 | 0.782(1) | -0.001(1) | 0.295(1) | 0.013(4) | 0.780(1) | 0.000(1) | 0.2936(9) | 0.014(4) | 0.778(1) | 0.001(1) | 0.296(1) | 0.014(4) |
| O2 | 0.727(1) | 0.243(2) | 0.125(1) | 0.011(4) | 0.729(1) | 0.241(1) | 0.125(1) | 0.011(4) | 0.7306(9) | 0.239(1) | 0.123(1) | 0.010(4) |
| O3 | 0.223(1) | 0.165(2) | 0.532(1) | 0.013(4) | 0.225(1) | 0.167(1) | 0.5286(9) | 0.014(4) | 0.228(1) | 0.169(1) | 0.526(1) | 0.013(4) |
| O4 | 0.266(1) | 0.852(2) | 0.296(1) | 0.013(4) | 0.2678(9) | 0.854(1) | 0.293(1) | 0.013(4) | 0.2694(9) | 0.853(1) | 0.295(1) | 0.013(4) |
| O5 | 0.261(1) | 0.056(1) | 0.100(1) | 0.014(4) | 0.2581(8) | 0.057(1) | 0.0985(8) | 0.014(4) | 0.2581(8) | 0.056(1) | 0.0983(8) | 0.015(4) |

*Notes:* Space group $P2_1/b$ (unique axis $a$). O5 is the site referred to as O/F by Friedrich et al. (2001). The O and F occupancies on O5 were fixed to 0.42 and 0.58, respectively. The occupancy of the M1 site was refined to the same value within 1 e.s.d. [Mg = 0.90(2); Fe = 0.10(2)] at all pressures.

**TABLE 7.** Atom positions and isotropic displacement parameters of the synthetic (OD,F)-chondrodite from neutron powder Rietveld refinements

| | 1.26 GPa | | | | 2.89 GPa | | | |
|---|---|---|---|---|---|---|---|---|
| | *x* | *y* | *z* | $U_{iso}$ | *x* | *y* | *z* | $U_{iso}$ |
| M1 | 1/2 | 0 | 1/2 | 0.0025(6) | 1/2 | 0 | 1/2 | 0.0034(7) |
| M2 | 0.013(2) | 0.1748(6) | 0.306(1) | 0.0025(6) | 0.010(2) | 0.1748(7) | 0.305(1) | 0.0034(7) |
| M3 | 0.495(2) | 0.8870(7) | 0.0796(9) | 0.0025(6) | 0.501(2) | 0.8860(8) | 0.079(1) | 0.0034(7) |
| Si | 0.0772(9) | 0.1417(6) | 0.703(1) | 0.006(1) | 0.0767(9) | 0.1410(6) | 0.706(1) | 0.004(1) |
| O1 | 0.775(1) | 0.0017(6) | 0.297(1) | 0.0049(6) | 0.774(2) | 0.0034(7) | 0.299(2) | 0.0063(7) |
| O2 | 0.732(1) | 0.2419(9) | 0.124(1) | 0.0049(6) | 0.729(2) | 0.2394(9) | 0.124(1) | 0.0063(7) |
| O3 | 0.225(1) | 0.1681(8) | 0.528(1) | 0.0049(6) | 0.223(2) | 0.1695(9) | 0.530(1) | 0.0063(7) |
| O4 | 0.267(1) | 0.8570(8) | 0.296(2) | 0.0049(6) | 0.266(1) | 0.8578(9) | 0.300(2) | 0.0063(7) |
| O5 | 0.263(2) | 0.058(1) | 0.103(1) | 0.008(2) | 0.263(2) | 0.059(1) | 0.106(1) | 0.002(2) |
| D | 0.108(3) | 0.022(2) | 0.019(3) | 0.040(4) | 0.103(4) | 0.022(2) | 0.020(3) | 0.030(4) |

| | 3.87 GPa | | | | 5.27 GPa | | | | 7.04 GPa | | | |
|---|---|---|---|---|---|---|---|---|---|---|---|---|
| | *x* | *y* | *z* | $U_{iso}$ | *x* | *y* | *z* | $U_{iso}$ | *x* | *y* | *z* | $U_{iso}$ |
| M1 | 1/2 | 0 | 1/2 | 0.0013(5) | 1/2 | 0 | 1/2 | 0.0022(6) | 1/2 | 0 | 1/2 | 0.0007(6) |
| M2 | 0.011(2) | 0.1746(6) | 0.3050(9) | 0.0013(5) | 0.011(2) | 0.1750(7) | 0.303(1) | 0.0022(6) | 0.012(2) | 0.1746(7) | 0.304(1) | 0.0007(6) |
| M3 | 0.493(2) | 0.8858(7) | 0.0786(8) | 0.0013(5) | 0.494(1) | 0.8864(7) | 0.0781(9) | 0.0022(6) | 0.497(2) | 0.8878(7) | 0.0787(9) | 0.0007(6) |
| Si | 0.0769(8) | 0.1407(6) | 0.704(1) | 0.003(1) | 0.0775(8) | 0.1409(6) | 0.702(1) | 0.001(1) | 0.0770(9) | 0.1419(6) | 0.705(1) | 0.001(1) |
| O1 | 0.771(1) | 0.0022(6) | 0.295(1) | 0.0052(6) | 0.773(1) | 0.0022(7) | 0.296(1) | 0.0052(7) | 0.774(1) | 0.0028(7) | 0.294(1) | 0.0030(6) |
| O2 | 0.731(1) | 0.2413(8) | 0.124(1) | 0.0052(6) | 0.729(1) | 0.2411(9) | 0.123(1) | 0.0052(7) | 0.735(2) | 0.2391(9) | 0.123(1) | 0.0030(6) |
| O3 | 0.227(1) | 0.1685(8) | 0.5278(9) | 0.0052(6) | 0.227(1) | 0.1692(9) | 0.525(1) | 0.0052(7) | 0.225(1) | 0.1696(9) | 0.525(1) | 0.0030(6) |
| O4 | 0.2676(9) | 0.8565(8) | 0.297(2) | 0.0052(6) | 0.268(1) | 0.8565(9) | 0.296(2) | 0.0052(7) | 0.268(1) | 0.8565(9) | 0.295(2) | 0.0030(6) |
| O5 | 0.262(2) | 0.059(1) | 0.103(1) | 0.006(2) | 0.264(2) | 0.0572(9) | 0.101(1) | 0.002(1) | 0.261(2) | 0.057(1) | 0.100(1) | 0.006(2) |
| D | 0.099(3) | 0.021(2) | 0.024(2) | 0.031(3) | 0.105(3) | 0.015(2) | 0.024(3) | 0.038(4) | 0.102(4) | 0.021(2) | 0.027(3) | 0.037(4) |

*Note:* Space group $P2_1/b$ (unique axis *a*).

**TABLE 8.** Selected interatomic distances (Å) and angles (°) associated with the D-atom environment in synthetic (OD,F)-chondrodite

| | 1.26 GPa | 2.89 GPa | 3.87 GPa | 5.27 GPa | 7.04 GPa |
|---|---|---|---|---|---|
| O5-D | 0.97(2) | 1.00(2) | 0.98(2) | 0.96(2) | 0.93(2) |
| O5···O5 | 2.99(2) | 3.00(2) | 2.97(2) | 2.95(2) | 2.91(2) |
| D···F* | 2.03(2) | 2.02(2) | 2.00(2) | 2.00(2) | 1.99(2) |
| O5-D···F* | 166(2) | 167(2) | 171(2) | 171(2) | 173(2) |
| O5···O1 | 2.99(1) | 3.02(1) | 2.96(1) | 2.94(1) | 2.90(2) |
| D···O1 | 2.47(2) | 2.48(2) | 2.49(2) | 2.49(3) | 2.48(2) |
| O5-D···O1 | 114(2) | 113(1) | 109(1) | 108(2) | 108(2) |
| D···D | 1.12(3) | 1.07(3) | 1.04(3) | 1.06(3) | 1.07(4) |

*The O5 site is occupied by 0.45 O + 0.55 F. Due to local ordering, however, D···O bonds are not possible for this hydrogen bond configuration. Refer to text for a more detailed discussion.

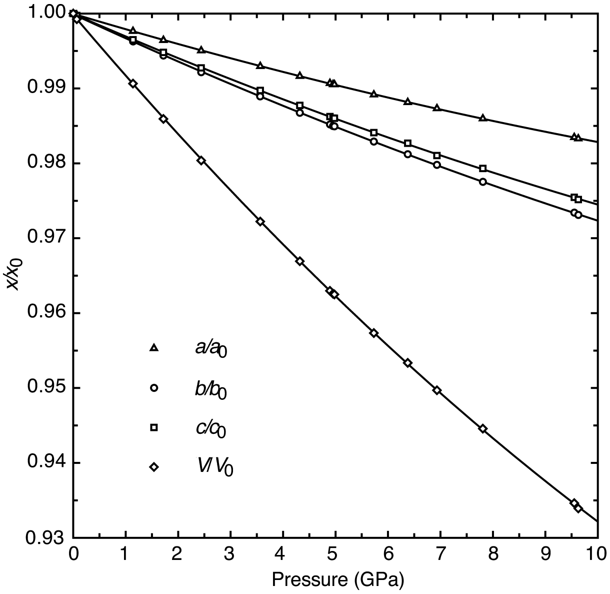

**FIGURE 3.** Variation of normalized cell parameters and unit-cell volume for the Tilly Foster chondrodite as a function of pressure.

obtained by Faust and Knittle (1994). Unfortunately, the OH content was not reported in their study.

The axial compressibilities show anisotropic behavior (Fig. 3), as described previously (Ross and Crichton 2001; Kuribayashi et al. 1998). The *a* axis is least compressible, showing a significantly different behavior than the *b* and *c* axes. In contrast to the hydroxylchondrodite (Ross and Crichton 2001), the Tilly Foster chondrodite, as well as the F-bearing chondrodite reported by Kuribayashi et al. (1998), show a slight difference between the compressibilities of the *b* and the *c* axes, with the *b* axis being the more compressible.

The variation of the normalized unit-cell parameters with pressure can be described by second-order polynomial equations:

$a/a_0 = 1.00000(2)\ \text{Å} - 2.09(1) \times 10^{-3}\ \text{Å GPa}^{-1} \times P + 3.8(1) \times 10^{-5}\ \text{Å GPa}^{-2} \times P^2$

$b/b_0 = 0.9998(2)\ \text{Å} - 3.2(1) \times 10^{-3}\ \text{Å GPa}^{-1} \times P + 4.5(1.1) \times 10^{-5}\ \text{Å GPa}^{-2} \times P^2$

$c/c_0 = 0.99999(5)\ \text{Å} - 3.05(2) \times 10^{-3}\ \text{Å GPa}^{-1} \times P + 5.1(2) \times 10^{-5}\ \text{Å GPa}^{-2} \times P^2$

The pressure dependencies of the *a* and *c* axes are significantly non-linear as indicated by the $P^2$ terms being more than 10 times their e.s.d.s. The behavior of the *b* axis is also clearly non-linear. The use of a higher order polynomial does not improve the fit and gives coefficients of the same magnitude as the uncertainties.

## X-ray structural refinements at high pressure

The structural changes that occur at high pressure are most easily interpreted in terms of the behavior of individual polyhedra. The $SiO_4$ tetrahedron is relatively incompressible whereas the $MO_6$ octahedra tend to become smaller and more regular (within standard deviations) at higher pressures, as can be seen by the quadratic elongation parameters (Table 5). The high-pressure behavior of F-bearing chondrodite is similar to that observed in forsterite, which has a structure closely related to that of the humites (Hazen 1976; Hazen and Finger 1980; Kudoh and Takéuchi 1985). The largest differences in polyhedral volume, as well as bond lengths, and intra- and inter-polyhedral bond angles with pressure occur in the M2 octahedron. This is not surprising as the M2 octahedron is located at the flexion points of the serrated octahedral chains (Fig. 4) and has the largest polyhedral volume at ambient conditions. The M1 octahedron shares edges with M2 and M3 octahedra within the (100) plane and with $SiO_4$ tetrahedra above and below this plane. Therefore, it is constrained within the polyhedral framework. The M3 octahedron is surrounded by three edge-sharing octahedra (M1, M2, M3) within the (100) plane, resulting in a rather symmetric bonding pattern. In contrast, the environment of the M2 octahedron is asymmetric in terms of the edges shared with M1 and M3 octahedra and the Si tetrahedron above (or below) (Fig. 4). Therefore, cation-cation repulsion between the asymmetrically arranged neighbors (M cations) distorts the M2 octahedron and moves the cation off-center in a direction away from the octahedral chain. As a result of this off-centering, the M2 octahedron has the two longest M-O bond distances [M2-O2 = 2.25(1) Å, M2-O3 = 2.20(1) Å] in the chondrodite structure (Table 5). These long bonds are most easily compressed, since the energy required to shorten a strained bond is less than what is needed to compress a relaxed bond by the same amount. Because the two long bonds are approximately parallel to the *b* axis, the largest compressibility is parallel to this direction. The displacement of the M2 cation also affects the intra- and inter-polyhedral bond angles; in particular those associated with anions at the O3 and O5 positions. For example, the Si-O3-M2 inter-polyhedral angle within the (100) plane is reduced by 2.1(3)°, indicating a kinking between corner-sharing $SiO_4$ tetrahedra and $M2O_6$ octahedra. The largest change of +3.8(5)° with pressure occurs for the M2-O3-M2 angle, which connects a (100) layer with the layer above and below, respectively. The pressure-induced increase of this angle could account for the stiffness of the *a* axis.

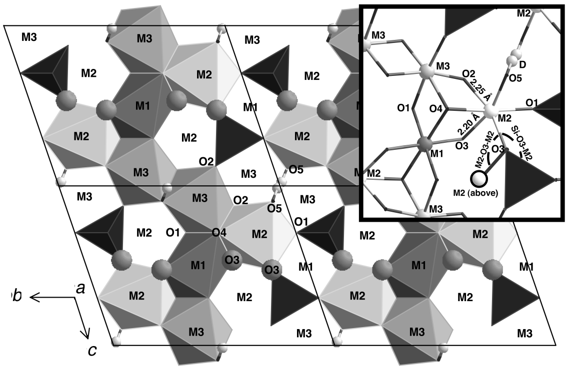

**FIGURE 4.** The [100] projection of the crystal structure of (OD,F)-chondrodite at ambient conditions. Small white spheres represent D sites; darker spheres O3 sites. The two D sites shown at the origin of the unit cell are related by a center of symmetry and are never occupied simultaneously. The inset highlights the bond distances and angles most affected on compression, as discussed in the text.

### O-D···O/F bond geometry at high pressure

In (OD,F)-chondrodite the D-atom is located adjacent to a center of symmetry between two O5 sites, and forms an asymmetric bifurcated hydrogen bond to O5 and O1 as acceptors (Fig. 5). The situation is further complicated by a disordered occupation of O5 by O- and F-atoms, which leads to three possible configurations (O-D···F, F···D-O, and F···F). The two centrosymmetrically related D sites are never occupied simultaneously (D site occupancy ≤50%), since this would lead to crystal-chemically unreasonable D···D distances (<1 Å) (Friedrich et al. 2001). Thus, when OH ≤1 pfu and (OH + F) = 2 pfu, an OD group is always adjacent to an F atom (on the O5 site) in the local environment, since for bond-valence reasons an F-D bond is not possible. Therefore, an O-D···O hydrogen bond is only formed with the oxygen atom at the O1 site.

The changes that occur in the O-D···O/F bond geometry (Table 8) at high pressures can be interpreted in terms of a rotation of the O-D vector into the cavity surrounding the D atom (Fig. 6). As a result of this rotation, the straight angle (O-D···F) widens and the bent angle (O-D···O) becomes narrower. In addition, the D···F hydrogen bond decreases slightly in length from 2.03(2) Å at 1.26 GPa to 1.99(2) Å at 7.04 GPa, which is consistent with a small decrease in the O5···O5 distance. In contrast, the D···O1 distance remains constant because the increase in length due to rotation of the O-D vector is apparently compensated for by compression of the O5···O1 distance.

The O-D distance remains relatively constant as a function of pressure, as observed in several neutron powder diffraction studies (e.g., Parise et al. 1994; Kagi et al. 2000). With the exception of the 7.04 GPa refinement, O-D distances vary within about one standard deviation. The significance of the decrease from 5.27 to 7.04 GPa [0.96(2) to 0.93(2) Å] is difficult to evaluate without additional data at higher pressure. As discussed above, the O5 site acts as both donor (O) and accep-

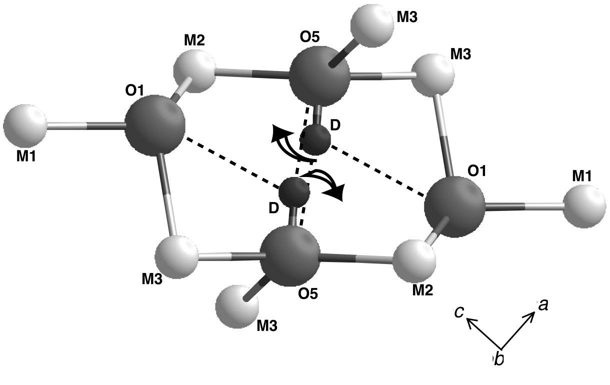

**FIGURE 5.** The O5-D···O5/O1 bond geometry in (OD,F)-chondrodite. Hydrogen bonds are indicated by dashed lines. The direction of the rotation of the O-D vector is represented by arrows.

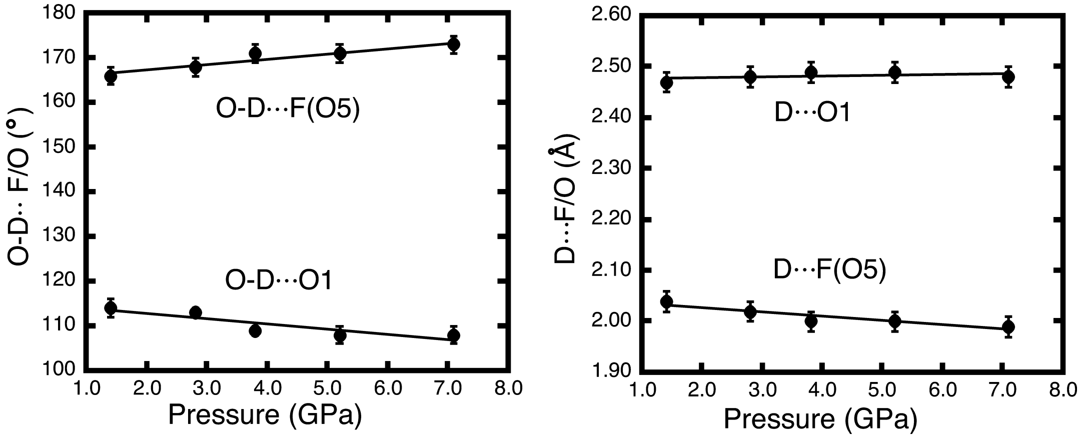

**FIGURE 6.** Variation of hydrogen bond angles and distances in (OD,F)-chondrodite as a function of pressure.

tor (F) in the hydrogen bond interaction in F-bearing chondrodite. This gives rise to a static disorder in the O5 position, which is reflected by a relatively long O-H distance [1.028(4) Å in F-bearing chondrodite (Friedrich et al. 2001) vs. 0.969(1) Å for the mean value determined from neutron diffraction studies (Ceccarelli et al. 1981)]. A small decrease in this apparent distance might be expected at high pressure as the degree of static disorder of the O5 atom becomes less in response to a shortening of the hydrogen bond distance.

### Correlation of crystallographic and spectroscopic measurements

Infrared- and Raman-spectroscopic data for F-bearing chondrodite (Williams 1992; Kuribayashi et al. 1998; Lin et al. 1999) have shown both positive and negative shifts of hydroxyl stretching vibrations with pressure. The shifts have been variously attributed to H-H repulsion (Williams 1992), O···O shortening (Kuribayashi et al. 1998), elongation of hydrogen bonds (Lin et al. 1999), O-H bond compression (Cynn and Hofmeister 1994; Hofmeister et al. 1999), and bending of the O-H···O angle as discussed for phase B, $Mg_{12}{}^{VI}Si^{IV}Si_3O_{19}(OH)_2$ (Hofmeister et al. 1999).

However, as mentioned above and previously noted by Lager et al. (2001), the interpretation with respect to H-H repulsion is not consistent with crystallographic data. Short H-H distances (<1 Å) are only an artifact of the average structure determined by diffraction methods and do not exist in the local structure probed by spectroscopic methods.

Based on the results of this study, the positive pressure shifts in the OH vibrational frequencies of F-bearing chondrodite up to at least 7 GPa cannot be due either to a lengthening of hydrogen bonds, or to increased H-H repulsion. Although the decrease in the length of the D···F hydrogen bond is only slightly larger than 2 e.s.d.s, the change is consistent with the shortening of the O5···O5 distance and the increase in the O-D···F angle. Without data at higher pressures, and in view of the disordered O5-D···O5 interaction, it is more difficult to evaluate the proposal by Hofmeister et al. (1999) that positive pressure shifts could be related to O-H bond compression. Nevertheless, the decrease in the O-D bond length at 7.04 GPa is consistent with this interpretation. Higher precision neutron data and single-crystal spectroscopic measurements at high pressure are required to unambiguously resolve the origin of these shifts as well as the differences observed among F-bearing chondrodites.

## ACKNOWLEDGMENTS

A.F. was financially supported by the Swiss National Science Foundation (Credit 21-052682.97 to M. Kunz). G.A.L. acknowledges support from the National Science Foundation through grant EAR-0073734. We thank the ISIS Neutron Facility, CLRC Rutherford Appleton Laboratory for neutron beam time, materials and other resources, and D.J. Francis for technical support on PEARL/HiPr. The authors also thank R. Miletich for experimental and technical support.

## REFERENCES CITED

Angel, R.J., Allan, D.R., Miletich, R., and Finger, L.W. (1997) The use of quartz as an internal pressure standard in high pressure crystallography. Journal of Applied Crystallography, 30, 461–466.

Aoki, K., Fujino, K., and Akaogi, M. (1976) Titanochondrodite and titanoclinohumite derived from the upper mantle in the Buell Park kimberlite, Arizona, USA. Contributions to Mineralogy and Petrology, 56, 243–253.

Baerlocher, C. (1993) Restraints and constraints in the Rietveld refinement. In R.A. Young, Ed., The Rietveld Method, International Union of Crystallography Monograph, 5, 186–196. Oxford University Press, U.K.

Besson, J.M., Nelmes, R.J., Hamel, G., Loveday, J.S., Weill, G., and Hull, S. (1992) Neutron powder diffraction above 10 GPa. Physica B, 180 and 181, 907–910.

Blessing, R.H. (1987) Data reduction and error analysis for accurate single crystal diffraction intensities. Crystallography Reviews, 1, 3–58.

Bohlen, S.R., Essene, E.J., and Boettcher, A.L. (1980) Reinvestigation and application of olivine-qtz-opx barometry. Earth Planetary Science Letters, 47, 1–10.

Bose, K. and Ganguly, J. (1995) Quartz-coesite transition revisited: Reversed experimental determinations at 500–1200 °C and retrieved thermochemical properties. American Mineralogist, 80, 231–238.

Burnham, C.W. (1966) Computation of absorption corrections and the significance of end effects. American Mineralogist, 51, 159–167.

Catti, M., Ferraris, G., Hull, S., and Pavese, A. (1995) Static compression and H disorder in brucite, $Mg(OH)_2$, to 11 GPa: A powder neutron diffraction study. Physics and Chemistry of Minerals, 22, 200–206.

Ceccarelli, C., Jeffrey, G.A., and Taylor, R. (1981) A survey of O-H...O hydrogen bond geometries determined by neutron diffraction. Journal of Molecular Structure, 70, 255–271.

Creagh, D.C. and McAuley, W.J. (1992) X-ray dispersion correction. In Wilson A.J.C., Ed., International Tables for Crystallography, vol. C, p. 206–219. Kluwer Academic Publishers, Dordrecht.

Cynn, H. and Hofmeister, A.M. (1994) High pressure IR spectra of lattice modes and OH vibrations in Fe-bearing wadsleyite. Journal of Geophysical Research, 99, 17717–17727.

Duffy, C.J. and Greenwood, H.J. (1979) Phase equilibria in the system $MgO-MgF_2-SiO_2-H_2O$. American Mineralogist, 64, 1156–1174.

Dymek, R.F., Boak, J.L., and Brothers, S. (1988) Titanian chondrodite- and clinohumite-bearing metadunite from the 3800 Ma Isua supracrustal belt, West Greenland: Chemistry, petrology and origin. American Mineralogist, 73, 547–558.

Engi, M. and Lindsley, D.H. (1980) Stability of titanian clinohumite: Experiments and thermodynamic analysis. Contributions to Mineralogy and Petrology, 72, 415–424.

Evans, B.W. and Trommsdorff, V. (1983) Fluorine hydroxyl titanianclinohumite in Alpine recrystallized garnet peridotite: Compositional controls and petrologic significance. American Journal of Science, 283A, 355–369.

Faust, J. and Knittle, E. (1994) Static compression of chondrodite: Implications for water in the upper mantle. Geophysical Research Letters, 21, 1935–1938.

Faust, J. and Williams, Q. (1996) Infrared spectra of phase B at high pressure: Hydroxyl bonding under pressure. Geophysical Research Letters, 23, 427–430.

Finger, L.W. and Prince, E. (1975) A system of Fortran IV computer programs for crystal structure computations. United States National Bureau of Standards, NBS Technical note, 854, Washington, D.C.

Finger, L.W. and King, H.E. (1978) A revised method of operation of the single-crystal diamond cell and refinement of the structure of NaCl at 32 kbar. American Mineralogist, 63, 337–342.

Friedrich, A., Lager, G.A., Kunz, M., Chakoumakos, B.C., Smyth, J.R., and Schultz, A.J. (2001) Temperature-dependent single-crystal neutron diffraction study of natural chondrodite and clinohumites. American Mineralogist, 86, 981–989.

Grant, D.F. and Gabe, E.J. (1978) The analysis of single-crystal Bragg reflections from profile measurements. Journal of Applied Crystallaography, 11, 114–120.

Hazen, R.M. (1976) Effects of temperature and pressure on the crystal structure of forsterite. American Mineralogist, 61, 1280–1293.

Hazen, R.M. and Finger, L.W. (1980) Crystal structure of forsterite at 40 kbar. Carnegie Institute Washington Year Book, 79, 364–367.

Hirth, G. and Kohlstedt, D.L. (1996) Water in the oceanic upper mantle: Implications for rheology, melt extraction and the evolution of the lithosphere. Earth and Planetary Science Letters, 144, 93–108.

Hofmeister, A.M., Cynn, H., Burnley, P.C., and Meade, C. (1999) Vibrational spectra of dense, hydrous magnesium silicates at high pressure: Importance of the hydrogen bond angle. American Mineralogist, 84, 454–464.

Kagi, H., Parise, J.B., Cho, H., Rossman, G.R., and Loveday, J.S. (2000) Hydrogen bonding interactions in phase A [$Mg_7Si_2O_8(OH)_6$] at ambient and high pressure. Physics and Chemistry of Minerals, 27, 225–233.

King, H.E. and Finger, L.W. (1979) Diffracted beam crystal centering and its application to high-pressure crystallography. Journal of Applied Crystallography, 12, 374–378.

Kitamura, M., Kondoh, S., Morimoto, N., Miller, G.H., Rossman, G.R., and Putnis, A. (1987) Planar OH-bearing defects in mantle olivine. Nature, 328, 143–145.

Kudoh, Y. and Takéuchi, Y. (1985) The crystal structure of forsterite $Mg_2SiO_4$ under high pressure up to 149 kb. Zeitschrift für Kristallographie, 171, 291–302.

Kuribayashi, T., Kudoh, Y., and Akizuki, M. (1998) Single-crystal X-ray diffraction and FTIR spectra of chondrodite, $Mg_5Si_2O_8(OH,F)_2$ under high pressure to 6.0 GPa. 17th General Meeting of the International Mineralogical Association, Toronto, A44.

Lager, G.A., Ulmer, P., Miletich, R., and Marshall, W.G. (2001) O-D···O bond geometry in OD-chondrodite. American Mineralogist, 86, 176–180.

Larson, A.C. and Von Dreele, R.B. (1994) General Structure Analysis System. Los Alamos National Laboratory Report LAUR 86–748.

Lin, C.-C., Liu, L.-G., and Irifune, T. (1999) High-pressure Raman spectroscopic study of chondrodite. Physics and Chemistry of Minerals, 26, 226–233.

Lundgren, P. and Giardini, D. (1994) Isolated deep earthquakes and the fate of subduction in the mantle. Journal of Geophysical Research, 99, 15833–15842.

Marshall, W.G. and Francis, D.J. (2002) Attainment of near-hydrostatic compression conditions using the Paris-Edinburgh cell. Journal of Applied Crystallography, 35, 122–125.

Maslen, E.N., Fox, A.G., and O'Keefe, M.A. (1992) X-ray scattering. In Wilson A.J.C., Ed., International tables for crystallography, vol C, p. 476–509. Kluwer Academic Publishers, Dordrecht.

McGetchin, T.R., Silver, L.T., and Chodos, A.A. (1970) Titanclinohumite: a possible mineralogical site for water in the upper mantle. Journal of Geophysical Research, 75, 255–259.

Miletich, R., Allan, D.R., and Kuhs, W.F. (2000) High-pressure single crystal techniques. In R.M. Hazen and R.T. Downs, Eds., High-Temperature and High-Pressure Crystal Chemistry, 41, p. 445–520. Reviews in Mineralogy and Geochemistry, Mineralogical Society of America, Washington, D.C.

Miller, G.H., Rossman, G.R., and Marlow, G.E. (1987) The natural occurrence of hydroxide in olivine. Physics and Chemistry of Minerals, 14, 461–472.

Parise, J.B., Leinenweber, K., Weidner, D.J., Tan, K., and Von Dreele, R.B. (1994) Pressure-induced H bonding: Neutron diffraction study of brucite, $Mg(OD)_2$, to 9.3 GPa. American Mineralogist, 79, 193–196.

Ribbe, P.H. (1979) Titanium, fluorine, and hydroxyl in the humite minerals. American Mineralogist, 64, 1027–1035.

———(1980) The humite series and Mn-analogs. In P.H. Ribbe, Ed., Orthosilicates, 5, p. 231–274. Reviews in Mineralogy, Mineralogical Society of America, Washington, D.C.

Rietveld, H.M. (1969) A profile refinement method for nuclear and magnetic structures. Journal of Applied Crystallography, 2, 65–71.

Risold, A.C., Trommsdorff, V., and Grobéty, B. (2001) Genesis of ilmenite rods and palisades along humite-type defects in olivine from Alpe Arami. Contributions to Mineralogy and Petrology, 140, 619–628.

Robinson, K., Gibbs, G.V., and Ribbe, P.H. (1971) Quadratic elongation: a quantitative measure of distortion in coordination polyhedra. Science , 172, 567–570.

Ross, N.L. and Crichton, W.A. (2001) Compression of synthetic hydroxylclinohumite [$Mg_9Si_4O_{16}(OH)_2$] and hydroxylchondrodite [$Mg_5Si_2O_8(OH)_2$]. American Mineralogist, 86, 990–996.

Sinogeikin, S.V. and Bass, J.D. (1999) Single-crystal elastic properties of chondrodite: Implications for water in the upper mantle. Physics and Chemistry of Minerals, 26, 297–303.

Stalder, R. and Ulmer, P. (2001) Phase relations of a serpentine composition between 5 and 14 GPa: significance of clinohumite and phase E as water carriers into the transition zone. Contributions to Mineralogy and Petrology, 140, 670–679.

Sykes, D., Rossman, G.R., Veblen, D.R., and Grew, E.S. (1994) Enhanced H and F incorporation in borian olivine. American Mineralogist, 79, 904–908.

Taskaev, V.I. and Ilupin, I.P. (1990) Association of clinohumite and K-richterite in the kimberlite of Kollektivnaya pipe. Doklady Akademii Natsional'naya USSR 310 (3), 683–686.

Weiss, M. (1997) Clinohumite: A field and experimental study. A dissertation of the Swiss Federal Institute of Technology Zürich (ETH), Diss. ETH No. 12202.

Williams, Q. (1992) A vibrational spectroscopic study of hydrogen in high pressure mineral assemblages. In Y. Syono and M.H. Manghnani, Eds., High-Pressure Research: Application to Earth and Planetary Sciences, p. 289–296. Terra Publishing Company, American Geophysical Union. Washington, D.C.

MANUSCRIPT RECEIVED NOVEMBER 13, 2001
MANUSCRIPT ACCEPTED FEBRUARY 22, 2002
MANUSCRIPT HANDLED BY BRYAN CHAKOUMAKOS